INFLUENCES OF FREQUENCY AND TEMPERATURE ON THE FATIGUE BEHAVIOR OF PLAIN-WEAVE CARBON/EPOXY COMPOSITE MATERIAL WITH FLAW SUBJECTED TO PARTIALLY-REVERSED CYCLIC LOADING

Marc-Claudel Deluy[1], Anh Dung Ngo[2], Martine Dubé[3] and Rajamohan Ganesan[4]

[1, 2, 3]École de Technologie Supérieure, 1100 Notre-Dame West, Montreal, Quebec, Canada, H3C 1K3, Mechanical Engineering Department, Laboratoire de fabrication et de caractérisation de matériaux composites (LFCMC), Email: [1]marc-claudel.deluy.1@ens.etsmtl.ca, [2]anh-dung.ngo@etsmtl.ca, [3]martine.dube@etsmtl.ca

[4]Concordia University, 1455 de Maisonneuve Blvd. West, Montreal, Quebec Canada, H3G 1M8, Mechanical and Industrial Engineering Department, Concordia Centre for Composites (CONCOM), Email: r.ganesan@concordia.ca

Keywords: Carbon-fiber, Composites, Fatigue, Temperature, Tension-compression

ABSTRACT

The objective of the present work is to study the fatigue behavior of a quasi-isotropic carbon/epoxy plain weave composite subjected to a partially-reversed cyclic load. Each of the tested composite coupons (3 in x 12 in) contains an artificial Teflon flaw (0.5 in x 0.5 in) in order to determine the flaw growth threshold, or delamination onset. The coupons were tested under different thermal-dry and loading frequencies conditions at different load levels. In total, four testing conditions were set: 1) 22-25°C-7 Hz (RTD7), 2) 82°C-7 Hz (ETD7), 3) 82°C-15 Hz (ETD15) and 4) 121°C-7 Hz (HTD7). Based on the experimental results, it was shown that increasing the temperature between RTD7, ETD7 and HTD7 conditions drastically reduced the delamination onset fatigue life of the coupon at a given stress level. Furthermore, the maximum allowable strain criteria for the delamination flaw growth threshold decreased as the operating temperature was increased between each condition. For the tested coupons at ETD condition, increasing the cyclic loading frequency from 7 Hz to 15 Hz enhanced the fatigue life at high stress levels and lowered the fatigue life at lower stress levels. A comparison was made with the results of similar tests from a previous research carried out in tension-tension (R = 0.1) fatigue loading [1, 2]. The present results showed significant decrease in fatigue life when compression mode was added during the fatigue cyclic loading.

1 INTRODUCTION

Nowadays, composite materials, such as carbon-epoxy composites, make up a great portion of the aerospace materials used for aircraft design. They are increasingly used, not only for non-structural parts, but also for the more critical functional parts that make up the aircraft. They are materials that combine high strength, high modulus, low density and fatigue resistance. Although composite materials offer superior performance to metals in many applications, they are not free from damage, deterioration or breakage, especially when containing internal flaws. Under operational use, the aircraft can be affected by environmental factors such as temperature and atmospheric turbulence which in turn can generate heat and vibration within the structural materials. Those factors could negatively affect the material already containing a certain type of flaw. In the literature, there is a very limited amount of work that has explored the fatigue behavior of plain-weave carbon/epoxy composites with flaws that are subjected to partially-reversed cyclic loads.

Classical damage types caused by tension loading include fiber pull-out, fiber bridging, fiber/matrix debonding, matrix cracking and edge delamination [3]. During tension-tension cyclic loading, all of these damage types evolve together progressively depending on the level of cycles reached. First damage starts as transverse matrix cracking in plain-weave fill yarns. Damage further progresses as failure due to shear stresses occur within the warp yarns. Delamination then occurs

between the warp and fill yarns. After coupling, the previously formed cracks (caused by the increasingly high level of internal stress) trigger delamination between plies and within the warp yarns [4]. Damage caused by compression is influenced by the microstructural alignment, geometry and properties of all the materials constituents [5]. Compressive loading involves also many damage types, which include mainly microbuckling and kinking of the fibers [6-9]. Other types of compressive damage include elastic microbuckling, fiber crushing, longitudinal splitting and delamination buckling [10]. Fatigue life and endurance limits are greatly reduced as temperature is increased because the material properties are affected detrimentally in manners of swelling and contraction that cause residual stress [11-13]. The damage rate is expected to be greatly increased when involving compression, especially in a cyclic loading. The coupling of the tension- and compression- damage types in fatigue should deteriorate the material properties (residual strength, residual stiffness) further and faster than each of the loading types would do alone [14, 15].

The objective of this paper is to study the influence of the frequency and temperature on the fatigue behavior of a plain-weave composite with an artificial flaw that is subjected to partially-reversed loading and determine when the flaw growth threshold (delamination onset) occurs. A proper delamination onset criterion based on strain increase must be set during tension-compression tests in order to obtain S-N curves for various thermal conditions. The delamination onset criterion has to be validated though the use of ultrasonic C-Scan inspection and microscopic observation. The results obtained in tension-compression (T-C) are compared with a previous work done on tension-tension (T-T) behavior to observe the influence of compression on the fatigue life [1, 2].

2 EXPERIMENTAL PROCEDURE

The general experimental setup for the fatigue testing mainly consists of all the apparatus described in Figure 1, which are a high-speed capture camera, an environmental chamber, a LabVIEW video-extensometer software, a MTS testing machine and a Thermotron hygrothermal controller.

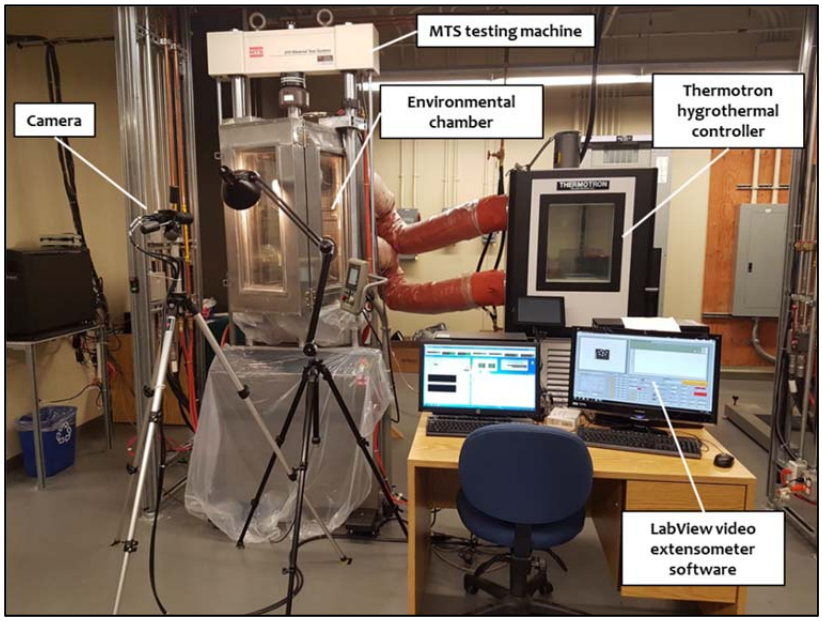

Figure 1: Experimental setup for the fatigue testing

2.1 Materials

Plain weave carbon/epoxy coupons manufactured by Bell Helicopter Textron Company (BHTC) were used for the fatigue testing in tension-compression (T-C). The thickness of each coupon is approximately 1.6 mm (0.0630 in) and the ply stacking configuration is [45/0/-45/90]s, totaling 8 plies per coupon. Each of the coupons contains a 2-layer Teflon insert located in-between the 3rd and 4th

plies in order to simulate an artificial flaw. The dimensions for the coupon and the Teflon insert are shown in Figure 2.

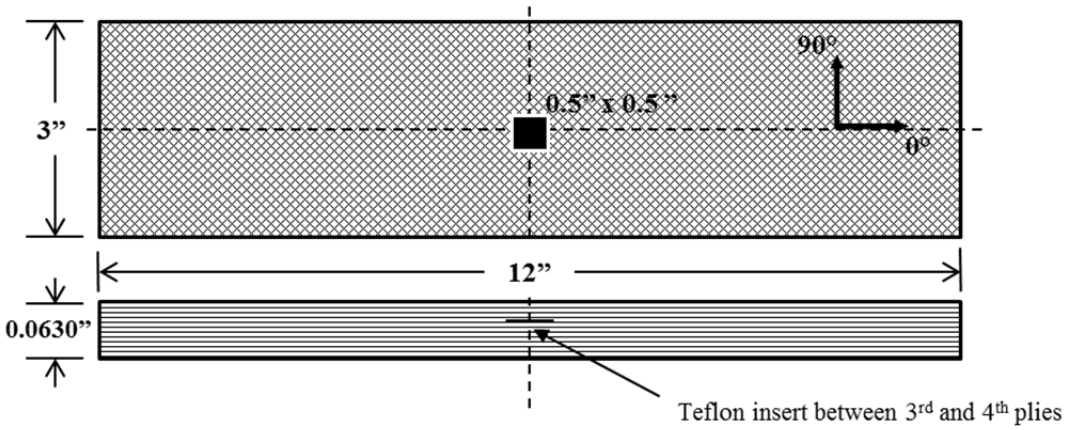

Figure 2: Plain-weave non-standardized test coupon with flaw and [45/0/-45/90]s stacking configuration

2.2 Mechanical testing

An MTS 810 servo-hydraulic testing machine was used to perform the fatigue tests in T-C. The machine standard equipment included a 100 kN load cell, an MTS 609 alignment system and hydraulic wedge grips (Figure 1). In order to avoid surface slipping between the grips and the coupons, aluminum end tabs and corrosion resistant stainless steel wire cloth were used. All fatigue tests were conducted in an environmental chamber in order to isolate the coupons from the laboratory environment and maintain constant and regulated temperature and humidity levels.

In Table 1, the parameters for each of the fatigue testing conditions are shown. A Thermotron hygrothermal controller was connected to the environmental chamber to control the temperature. Tests were conducted at room temperature (RT=22-25°C), elevated temperature (ET=82°C) and high temperature (HT=121°C). The relative humidity level was set to 0% (Dry) for each testing conditions, except for room temperature where it wasn't controlled.

The static ultimate tensile load (UTL) values [1] obtained from a previous study [1, 2] using the same coupons and thermal conditions were reused as a reference for the load levels in this work. The ultimate tensile stress (UTS) was calculated based on the maximum applied load and the coupon cross-sectional area. The load-controlled T-C fatigue tests were conducted at a partially-reversed stress ratio R of -0.1 and cyclic loading frequencies of 7 Hz and 15 Hz were chosen. Three coupons were used per load level for each condition, reaching a total of 39 coupons.

Condition	Temperature (°C)	Relative Humidity (%)	Frequency (Hz)	Load/UTL (%)
RTD7	22-25 (ambient)	Not controlled	7	63, 57, 51
ETD7	82.2	0% (Dry)	7	60, 55, 50
ETD15	82.2	0% (Dry)	15	60, 55, 50
HTD7	121.1	0% (Dry)	7	60, 50, 47.5, 45

Table 1: Partially-reversed T-C fatigue testing parameters

2.3 Anti-buckling fixture

A custom made anti-buckling fixture with an observation window (2 in x 3 in) was designed especially for the type of coupons used in order to avoid out-of-plane buckling during compression.

[1] Due to contractual requirements, actual data on UTL and UTS have to remain confidential.

The fixture inner contact surfaces were equipped with a ball-bearing system in order to reduce the heat due to surface friction. The anti-buckling fixture was rigidly attached to the top wedges with brackets in order to eliminate any rotational end movement of the fixture during the compressive tests. To guarantee that no buckling occurred between the bottom grips and lower part of the anti-buckling fixture, the gap was kept to 3 mm or less. The anti-buckling fixture is shown in Figure 3.

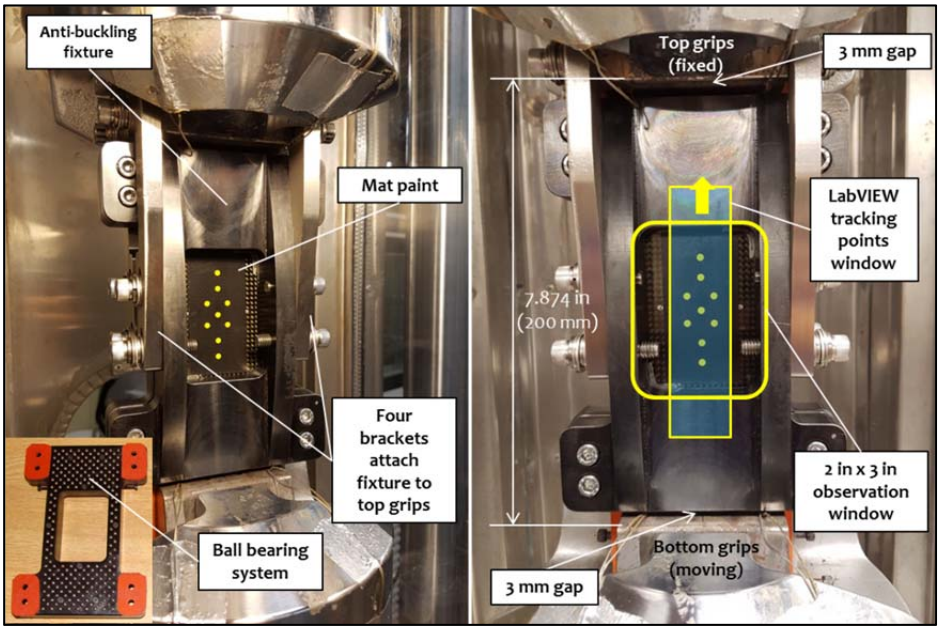

Figure 3: Anti-buckling fixture with observation window

2.4 LabVIEW video-extensometer software

A custom-made video-extensometer tool was designed in the National Instruments™ LabVIEW software in order to measure the strain around the Teflon artificial flaw in real time. It was connected to a camera with a capture capability of up to 300 frames per second. In order to achieve the measurements, a set of light-colored capture dots were placed around the artificial flaw region and along the longitudinal loading axis. The observation window in the anti-buckling fixture was purposely designed to allow such measurements. A thin layer of mat paint (Figure 3) was applied to increase the contrast between the coupons surface and the capture points. Figure 4 illustrates the set of tracking points surrounding the artificial flaw region, which were identified from P0 to P7. The points P0 and P1 were primarily used for longitudinal strain measurements and delamination onset criteria calculations. The dimensions of the tracking points are shown in Figure 4, where, for example, $D_{P0\text{-}P1}$ represents the distance between points P0 and P1.

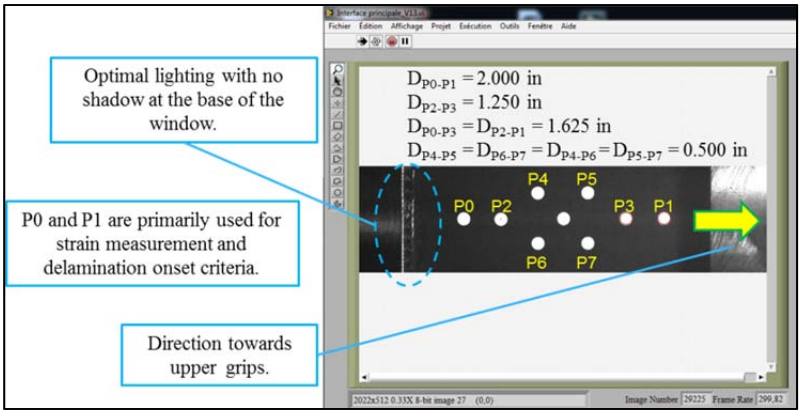

Figure 4: LabVIEW graphical user interface with tracking points

2.5 Determination of the fatigue delamination onset criterion

In order to determine the fatigue delamination onset, a strain increase criterion, or εCRT, was required. The criterion was used as an indicator to identify the damage initiation threshold surrounding the internal flaw leading to delamination in terms of longitudinal strain increase. Only the strain level for the tensile part of the applied cyclic load was accounted for during the calculation of the criterion. The criterion is defined in Equation 1 as:

$$\varepsilon CRT\ (\%) = 100 \cdot \left(\frac{\varepsilon_N - \varepsilon_{1000}}{\varepsilon_{1000}}\right) \tag{1}$$

where ε_{1000} and ε_N are the longitudinal strains at 1000 and N loading cycles, respectively.

For all conditions, 4 to 5 coupons were tested in fatigue at load levels varying between 50% and 63% UTL. The fatigue tests were conducted until a target value of εCRT was reached which ranged from 4% to 22% of strain increase among all conditions.

2.6 TecScan ultrasonic C-Scan

Before and after each fatigue test, the coupons were inspected using an ultrasonic immersive TecScan scanner and its TecView™ UT software. C-Scan inspections were conducted after fatigue tests in order to detect and observe damage in the vicinity of the artificial flaw. The obtained C-Scan imagery was then compared to pre-test C-Scans to monitor the damage progression. A V309 Panametrics piezoelectric transducer with a 0.5 inch diameter, a 2.0 inch point target focus (PTF) and 5.0 MHz nominal center frequency was used for each scan, where water was used as a medium. The dimension of the scan surface area surrounding the flaw region was 1.00 in x 2.25 in. The TecScan ultrasonic machine with C-Scan samples of before- and after- fatigue tests are shown in Figure 5.

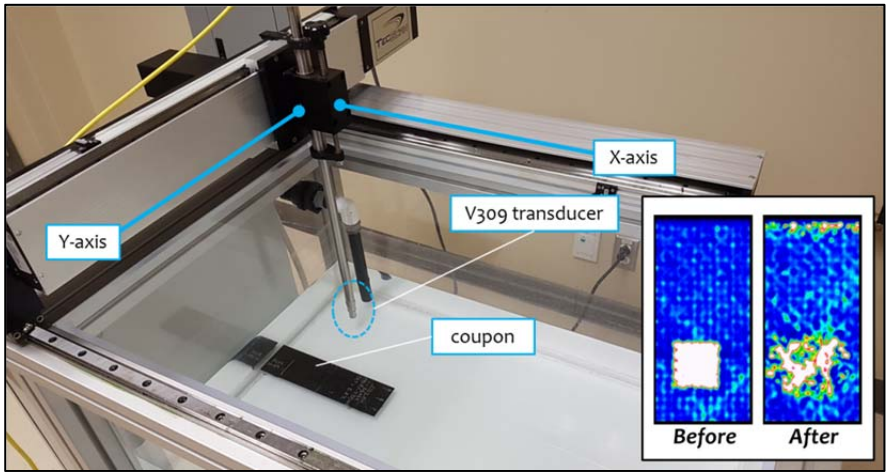

Figure 5: Ultrasonic immersive TecScan scanner with C-Scan samples

2.7 Microscopic observations

To further investigate the damage in the vicinity of the Teflon insert, a Clemex Captiva optical microscope was used. The coupons were cut around the Teflon insert into small 10 x 60 mm strips using a Dremel cutter equipped with a diamond saw blade. The strips' surfaces were polished using silicon carbide paper with grit indexes of 400, 600, 800 and 1000. Observations were made using an optical zoom of 50X (300 µm scale) on both sides of the strips in the vicinity of the Teflon flaw from top to bottom tips, as shown in Figure 6. The microscopic observations were made to validate the C-Scans inspection results and focused mostly on damage characterization.

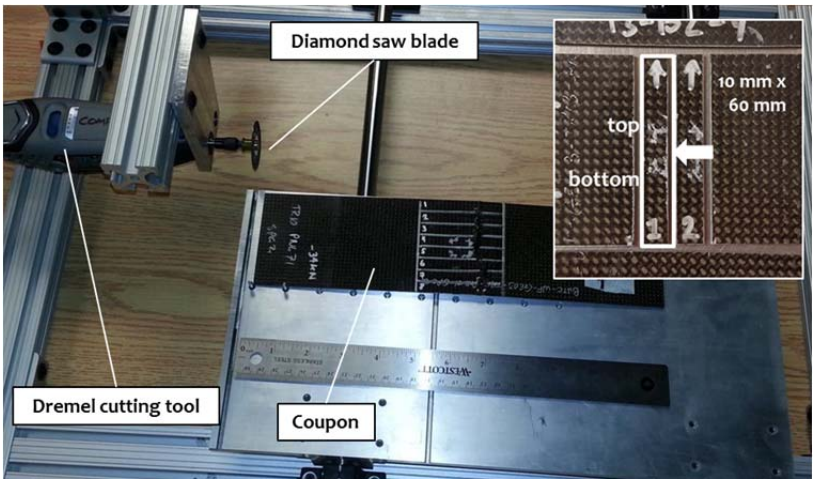

Figure 6: Coupons cutting setup

3 RESULTS AND DISCUSSION

3.1 Determination of the strain criterion: C-Scans and microscopy

For conditions RTD7, ETD7, ETD15 and HTD7, the strain criterion was determined by conducting T-C fatigue tests at 63%, 60%, 60% and 50% UTL, respectively. After each test, C-Scan inspections were conducted. Microscopic observations were made as well in order to validate to some degree the C-Scan results. Figure 7 presents the results obtained from the C-Scan inspections done on the damaged coupons after testing for all conditions. Starting with the RTD7 condition, tests ran until the strain increase criterion εCRT reached 5%, 10%, 15%, 19% and 22% by using 5 different coupons. At εCRT = 5%, results show that damage seems to be contained and very little propagation is visible. At εCRT = 10%, damage starts to appear at the bottom part of the flaw. Then, damage appears to increase from εCRT = 15% to εCRT = 19%. Between εCRT = 19% and εCRT = 22%, the damage level seems to be stabilizing. Based on the results, the εCRT associated to the delamination onset for RTD7 was chosen to be 10%. The corresponding εCRT values for the ETD7, ETD15 and HTD7 conditions were determined in the same manner. It is interesting to notice that the value of εCRT decreases as soon as temperatures are elevated or high while it slightly increases with the frequency.

Condition	C-Scans obtained after T-C testing w/ corresponding εCRT(%)				
RTD7 εCRT = 10.0% 63% UTL	5.0 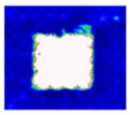	10.0 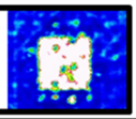	15.0 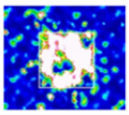	19.0 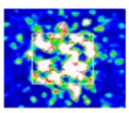	22.0 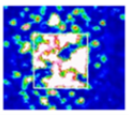
ETD7 εCRT = 6.0% 60% UTL	4.0 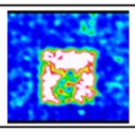	6.0 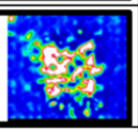	8.0 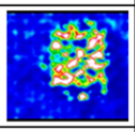	10.7 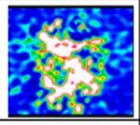	
ETD15 εCRT = 7.0% 60% UTL	5.0 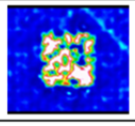	7.0 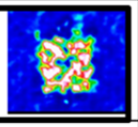	9.0 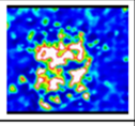	11.4 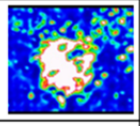	
HTD7 εCRT = 7.0% 50%UTL	4.7 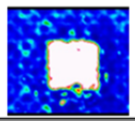	6.4 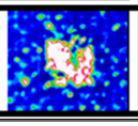	8.6 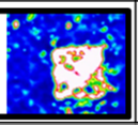	10.4 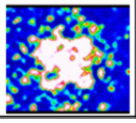	

Figure 7: After test C-Scans for all conditions with their respective strain increase εCRT criterion values

Figure 8 presents the evolution of damage related to the strain increase criterion. Microscopic observations were made for condition RTD7 at their respective εCRTs described before where the crack lengths were measured in the vicinity of flaw and both of its tips. The crack-tip-to-flaw propagation length ratio (CTF) is calculated in Equation 2 as follow:

$$CTF\ ratio\ (\%) = 100 \cdot \left(\frac{l_{crack\ tip}}{l_{flaw}}\right) \tag{2}$$

where $l_{crack\ tip}$ is the measured crack tip length and l_{flaw} is the measured flaw length (Teflon insert and air pockets). Between εCRT = 5% and εCRT = 10%, the CTF ratio increases slightly from 9% to 11%. By the time εCRT reaches 15%, the CTF ratio more than doubles, increasing from 11% to 23%. From εCRT = 10% onward, the CTF ratio increases almost linearly until it reaches 34%. Based on the CTF data behavior, the εCRT associated to the delamination onset for RTD7 was chosen to be 10%. These CTF ratio measurements validate the qualitative C-Scan observations and were made for the RTD7 condition only.

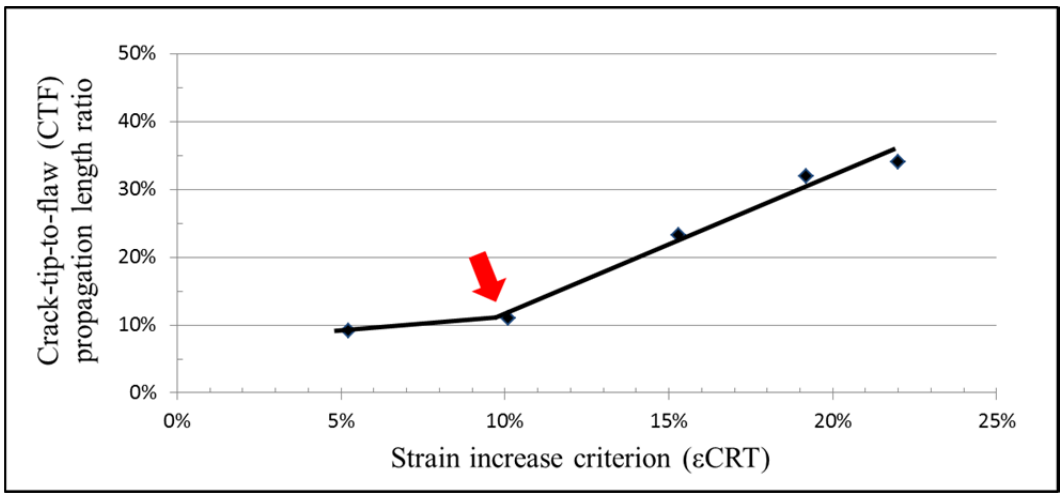

Figure 8: Strain increase influence on the flaw tip damage propagation for RTD7

Figure 9 illustrates the typical damage types encountered in condition RTD7. In Figure 9a, cracking occurs after a certain amount of strain increase and progresses under the form of delamination from the flaw tip. In Figures 9b-9e, four specific damage types are illustrated: longitudinal fill cracks, transversal fill cracks, inter-yarn delamination and inter-ply delamination. The first type of damage to occur seems to be the transversal fill yarn cracking due the tension part of the cyclic load (Figure 9c). Inter-yarn delamination then occurs due to the compressive stress levels that induce internal buckling delamination on the yarns and shear stress on their interface (Figure 9d). After subsequent T-C loading, the damage levels progress further within the plain-weave plies in the fill yarns under the following forms: longitudinal cracks due to compression (Figure 9b) and transversal cracks due to tension. When the density of the longitudinal and transversal cracks is critical, the damage progresses under the form of an inter-ply delamination (Figure 9e). It is safe to assume that the T-C fatigue mode (R=-0.1) induces faster damage rate when compared to the T-T fatigue mode (R = 0.1). It would seem that damage is sustained by the Teflon flaw's surrounding plies before crack initiation occurs at the tip. The yarns surrounding the Teflon flaw structurally weakens and could allow easier internal buckling that leads to flaw tip cracking and subsequent crack propagation.

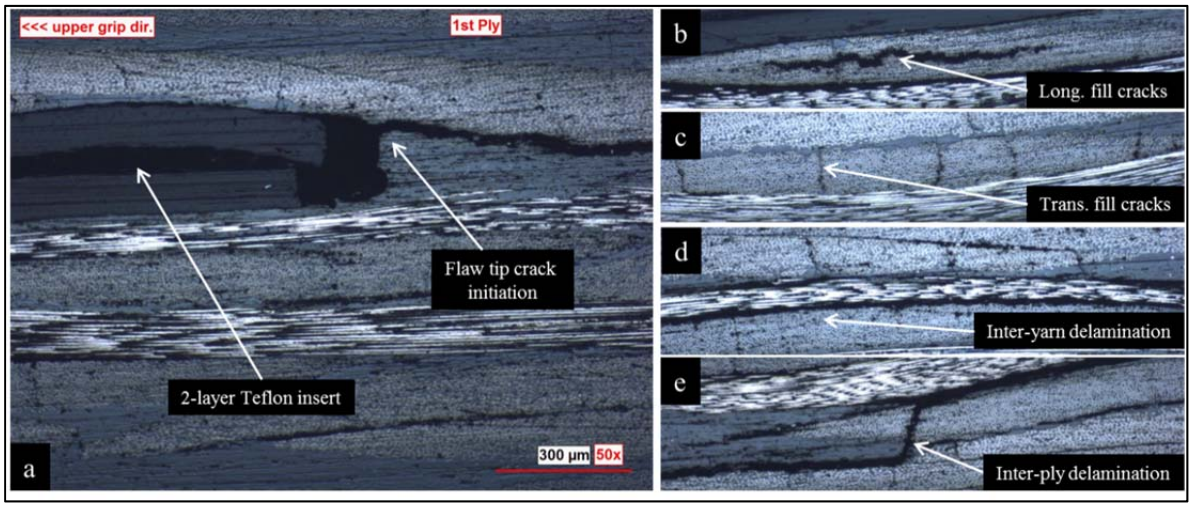

Figure 9: Micrographs showing delamination and damage types in the vicinity of the Teflon insert for RTD7 at εCRT = 10%. (a) Delamination initiation and growth from the flaw tip. (b) Longitudinal cracking in fill yarns (compression). (c) Transversal cracking in fill yarns (tension). (d) Inter-yarn delamination (warp & fill). (e) Inter-ply delamination.

3.2 Fatigue stress-cycle (S-N) curves

After the determination of the strain increase criterion was completed, fatigue tests were started to determine the delamination onset S-N curves. Based on the load-controlled levels described in Table 1, T-C fatigue tests were conducted for each condition until their respective delamination onset εCRT values were reached. To obtain the S-N curves, the fatigue tests were load-controlled and then converted to stress level $\sigma_{max}/\sigma_{UTS}$. A fatigue model was defined based on the obtained S-N regression lines:

$$\frac{\sigma_{max}}{\sigma_{UTS}} = a - b\log_{10}(N_{onset}) \tag{3}$$

where σ_{max} is the maximum value of the applied cyclic stress, σ_{UTS} is the ultimate tensile stress, a and b are parameters defined by the linear regression and N_{onset} is the number of cycles at the delamination onset. In Table 2 are described the parameters a and b for each condition. The parameters a and b represent the S-N curve stress level shift and slope, respectively.

Condition	Temp. (°C)	RH (%)	*f* (Hz)	a	b	R^2	εCRT(%)
RTD7	22-25	Not controlled	7	1.236	0.136	0.665	10.0
ETD7	82.2	0% (Dry)	7	1.249	0.143	0.906	6.0
ETD15	82.2	0% (Dry)	15	1.379	0.170	0.975	7.0
HTD7	121.1	0% (Dry)	7	0.926	0.106	0.986	7.0
HTD7	121.1	0% (Dry)	7	0.608	0.030	0.985	7.0

Table 2: Tension-compression S-N linear curve regression data results for all thermal conditions

In Figure 10 are presented the comparison of T-C and T-T fatigue S-N curves for condition RTD7. The T-T fatigue tests were realized at a cyclic stress ratio of 0.1 from a previous work [1]. The delamination onset εCRT value for both type of tests were equal at 10%. At room temperature, it is important to mention that the relative humidity was not controlled and that the ambient temperature was varying between 22°C and 25°C depending on the hour and day. Based on the results obtained, adding a compressive component to a cyclic load clearly deteriorates the delamination onset fatigue life compared to a pure tensile cyclic load. Since the b parameters are nearly equal in both T-C and T-T fatigue curves, for every drop of 5% in the UTS level, the discrepancy in the delamination onset

cycle number multiplies by a constant factor of about 2.368 between both. For example, at 60% UTS there is a discrepancy of nearly 218 800 cycles, at 55% UTS it is nearly 518 100 cycles, at 50% UTS it is nearly 1 226 800 and so on.

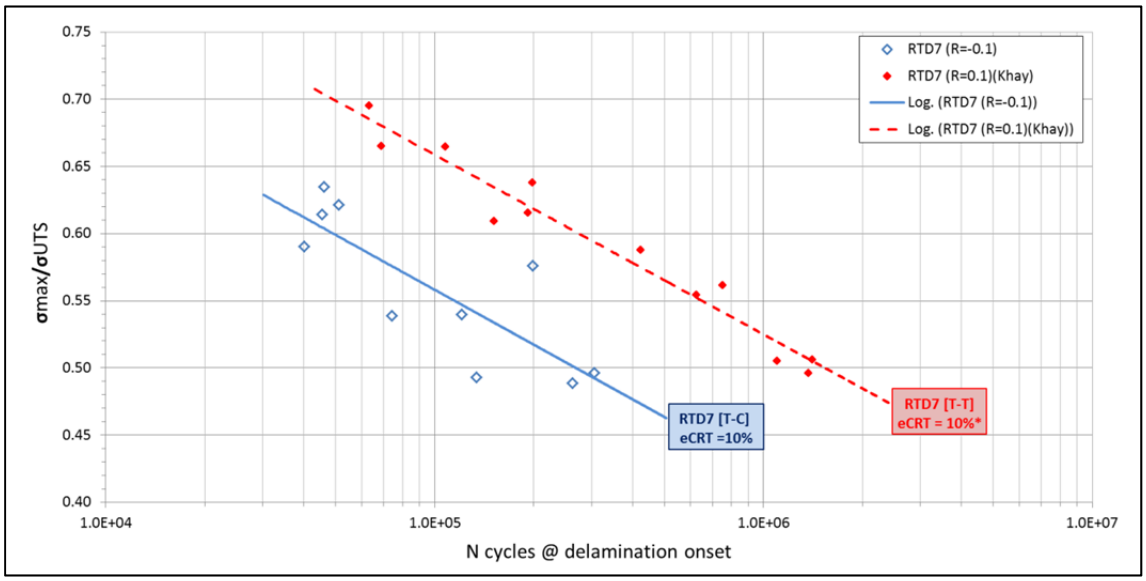

Figure 10: Comparison of the S-N curves in T-C and T-T [1] for condition RTD7

In Figure 11 are presented the comparison of the T-C and T-T fatigue S-N curves for conditions ETD7 and ETD15. Similar to condition RTD7, the fatigue life of the delamination onset for ETD7 is greatly deteriorated when compression is included in the cyclic loading. Since the slope of T-C is higher than T-T, the discrepancy factor will slightly decrease for every drop of 5%UTS, i.e., at 60% UTS there is a discrepancy of nearly 188 835 cycles, at 55% UTS the discrepancy factor is 3.096 (584 555 cycles), and at 50% UTS there is a discrepancy factor of 3.059 (1 788 001 cycles). For ETD15, the discrepancy factor is slightly decreasing from 2.529 to 2.517 for every drop in 5% UTS which is less than the ETD7 factor.

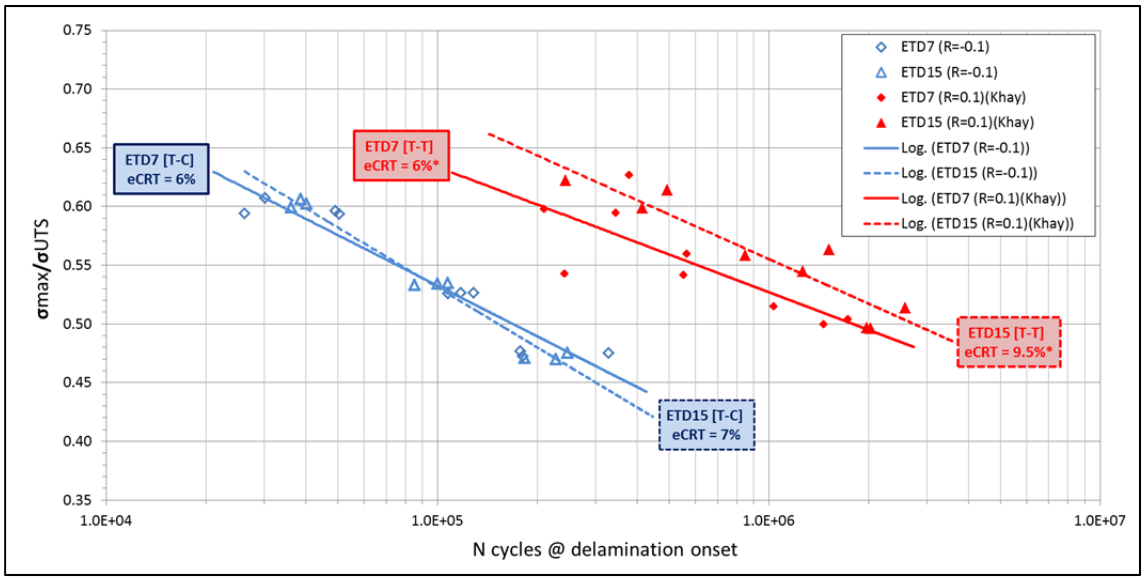

Figure11: Comparison of the S-N curves in T-C and T-T [1] for conditions ETD7 and ETD15

In Figure 12, all the delamination onset fatigue life S-N curves in T-C are compared. In the case of the HTD7 data points, it can be observed that there are only two points for 43%, 45.6% and 58.4% of

UTS. For each of these stress levels, one result fell far off the limit of the average and standard deviation was removed for that reason. Plus, the quantity of testing coupons was limited. From those data points, two S-N curves were found: the high slope curve (HTD7-SN1) has fatigue life range of about 1 000 to 20 000 cycles and the low slope curve (HTD7-SN2) has a range of 10 000 to 1 215 000 cycles.

The effect of temperature definitely deteriorates the delamination onset fatigue life of the coupons. This is mostly true for the condition HTD7. Since the slope of HTD7-SN1 is smaller than RTD7, the discrepancy factor decreases slightly with the stress level $\sigma_{max}/\sigma_{UTS}$ and its average is 2.310. For ETD7, its slope is higher than HTD7 and the discrepancy factor is about 2.201, decreasing slightly with the stress level. The slope of HTD7-SN2 seems to exhibit the behavior of an endurance limit. But to be able to confirm this theory, further damage stability inspection has to be conducted, whether it is by microscopic observation or residual strength testing. In the case of ETD7 and ETD15, both curves are crossing at approximately 56% UTS or 65 000 cycles. At high stress levels, the increase of frequency seems to enhance the delamination onset fatigue life while it deteriorates it at lower stress levels.

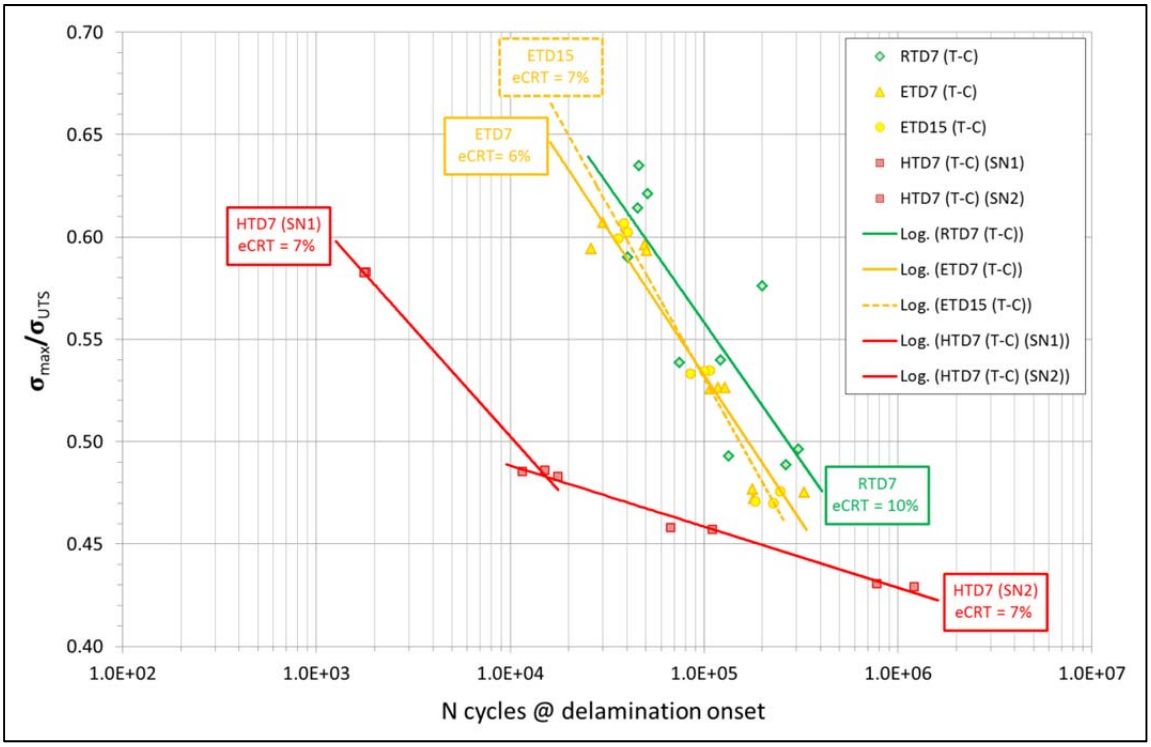

Figure 12: Comparison of the S-N curves in T-C for conditions RTD7, ETD7, ETD15 and HTD7

4 CONCLUSION

The conducted tests on the plain-weave carbon/epoxy composite with flaw have revealed the following results:

- The effects of a partially-reversed tension-compression cyclic loading on the delamination onset fatigue life testing are more damaging than the effects of a tension-tension cyclic load due to the complex interaction and evolution of the compressive and tensile types of damage.
- C-Scans showed that the delamination onset criterion εCRT decreases as soon as temperatures are elevated or high.
- Microscopic observation revealed that longitudinal cracking in fill yarns (compression), transversal cracking in fill yarns (tension), inter-yarn delamination (warp & fill) and inter-ply delamination were the main four types of damage.

- The effect of the temperature on a plain-weave composite accelerates the degradation of the material properties and consequently the fatigue life of the delamination onset. This is especially true for conditions where the temperature reaches more than 121.1°C.
- Increasing the frequency from 7Hz to 15Hz seems to enhance the fatigue life of the delamination onset at high stress level (60% UTS and more) while its decreases the fatigue life at lower stress levels (50% UTS or less).

ACKNOWLEDGEMENT

Special thanks to the Consortium for Research and Innovation in Aerospace in Québec (CRIAQ) and MITACS for the academic funding, the Natural Sciences and Engineering Research Council of Canada (NSERC), Bombardier Aerospace, Bell Helicopter Textron Company and L-3 MAS Communications.

REFERENCES

[1] M. Khay, A.D. Ngo, R. Ganesan, Frequency effect on fatigue tensile behaviour of carbon/epoxy plain weave laminates under different hygrothermal conditions. *In Canada-Japan-Vietnam Workshop on Composites, August 2016, Ho-Chi-Minh city, Vietnam*. 2016. pp. 9.

[2] M. Khay, M. Cardonne, P.L. Vachon, M. Dubé, R. Ganesan and A.D. Ngô, Experimental Investigation of the Tensile-Tensile Fatigue Behaviour of Carbon/Epoxy Plain Weave Laminates, *Proceedings of the Tenth Joint Canada-Japan Workshop on Composites, Vancouver, Canada, August 2014*, DEStech Publications, Inc., Design, Manufacturing and Applications of Composites, 2014. pp. 36-44.

[3] T.L. Anderson, *Fracture Mechanisms in Nonmetals*, Fracture mechanics: fundamentals and applications, 3rd Edition, Boca Raton: Taylor & Francis Group, LLC, 2005.

[4] N.K. Naik, *Woven-fibre thermoset composites*, Fatigue in Composites: Science and Technology of the Fatigue Response of Fibre-Reinforced Plastics, CRC Press, Boca Raton, 2003.

[5] A.M. Waas and R.S. Carl, Compressive failure of composites, Part II: Experimental studies, *Progress in Aerospace Sciences*, **32**, 1996, pp. 43-78.

[6] H. Thom, A review of the biaxial strength of fibre-reinforced plastics, *Composites Part A*, **29A**, 1998, pp. 869–886.

[7] B.W. Rosen, *Mechanics of composite strengthening*, Fiber Composite Materials, Chapter 3, ASM, Metals Park, Ohio, 1965.

[8] B. Budiansky, Micromechanics, *Computers & Structures*, **16**, 1983, pp. 3-12.

[9] B. Budiansky and N.A. Fleck, Compressive kinking of fiber composites: A topical review, *Applied Mechanics Reviews*, **47**, 1994, pp. 246-250.

[10] N.A. Fleck, Compressive failure of fiber composite, *Advances in Applied Mechanics*, **33**, 1997, pp. 43-117.

[11] R. Khan, Z. Khan, F. Al-Sulaiman and N. Merah, Fatigue life estimates in woven carbon fabric/epoxy composites at non-ambient temperatures, *Journal of Composite Materials*, **36**, 2002, pp. 2517-2534.

[12] T. Shimokawa, Y. Kakuta, D. Saeki, and Y. Kogo, Carbon plain-weave fabric low-temperature vacuum cure epoxy composite: static and fatigue strength at room and high temperatures and practicality evaluation, *Journal of Composite Materials,* **41**, 2007, pp. 2245-2265.

[13] M. Kawai and Y. Matsuda, Anisomorphic constant fatigue life diagrams for a woven fabric carbon/epoxy laminate at different temperatures, *Composites: Part A*, **43**, 2012, pp. 647–657.

[14] E.K. Gamstedt and B.A. Sjögren, Micromechanisms in tension-compression fatigue of composite laminates containing transverse plies, *Composites Science and Technology*, **59**, 1999, pp. 167-178.

[15] S. Mall, D.W. Katwyk, R.L. Bolick, A.D. Kelkar, and D.C. Davis. 2009, Tension–compression fatigue behavior of a H-VARTM manufactured unnotched and notched carbon/epoxy composite, *Composite Structures*, **90**, 2009, pp. 201–207.